Supplement of Atmos. Chem. Phys., 25, 18313–18323, 2025
https://doi.org/10.5194/acp-25-18313-2025-supplement
© Author(s) 2025. CC BY 4.0 License.

Atmospheric Chemistry and Physics
Open Access
EGU

Supplement of

Ethylamine-driven amination of organic particles: mechanistic insights via key intermediates identification

Peiqi Liu et al.

Correspondence to: Meirong Zeng (meirongzeng@sjtu.edu.cn)

The copyright of individual parts of the supplement might differ from the article licence.

Section S1. Supporting experimental data

This section presents supporting experimental data consisting of particle size distributions (Fig. S1), reaction products distributions (Figs. S2 and S3), kinetic profiles (Fig. S4), APPI-HRMS (Fig. S5), and uptake coefficients (Figs. S6 and S7).

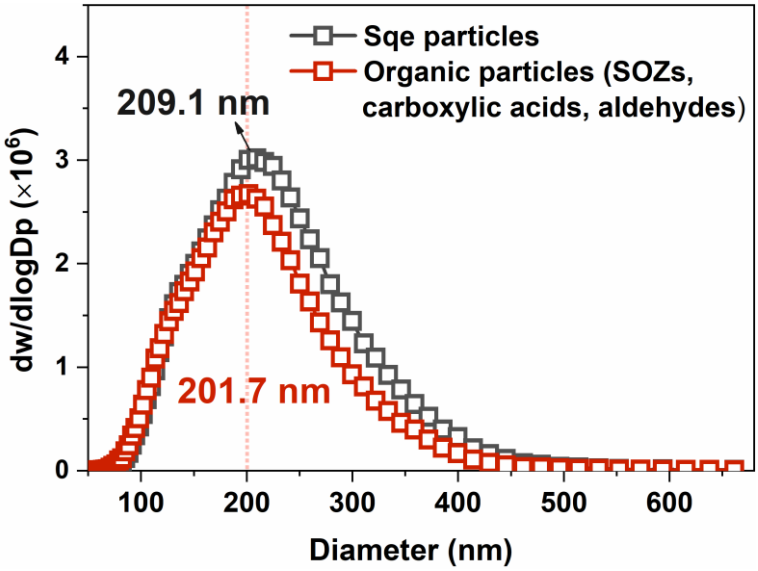

Figure S1. Size distributions of Sqe particles and organic particles measured by SMPS. The diameters of organic particles (201.7 nm) is comparable to that of Sqe particles (209.1 nm).

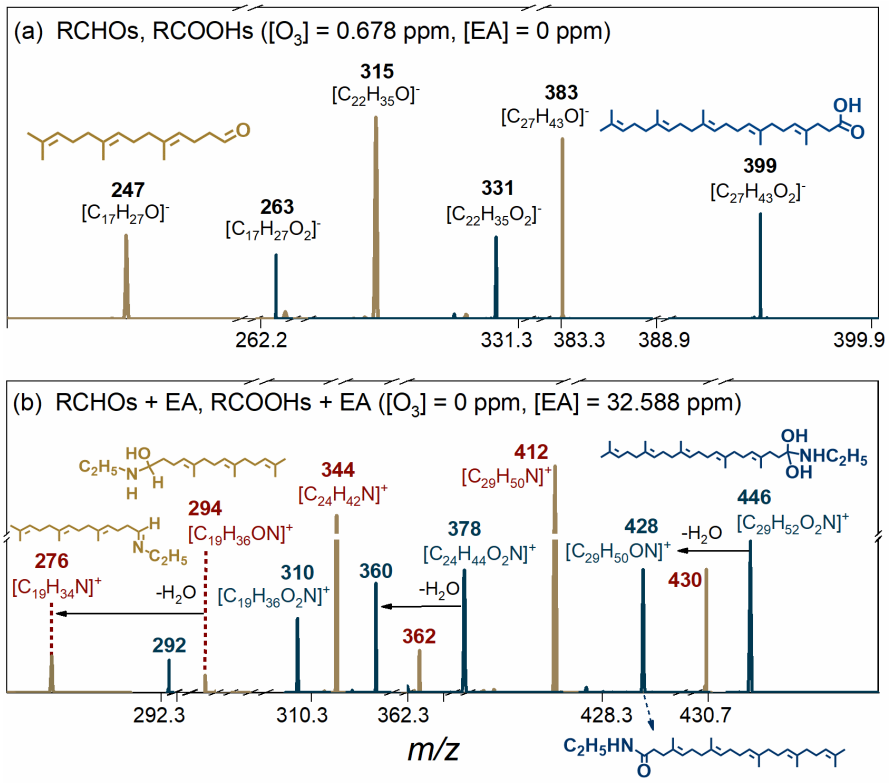

Figure S2. Mass spectra of (a) representative aldehydes (RCHOs) and carboxylic acids (RCOOHs) generated from Sqe ozonolysis in the first flowtube reactor, and (b) their amination products upon ethylamine (EA) exposure in the secondary flowtube reactor.

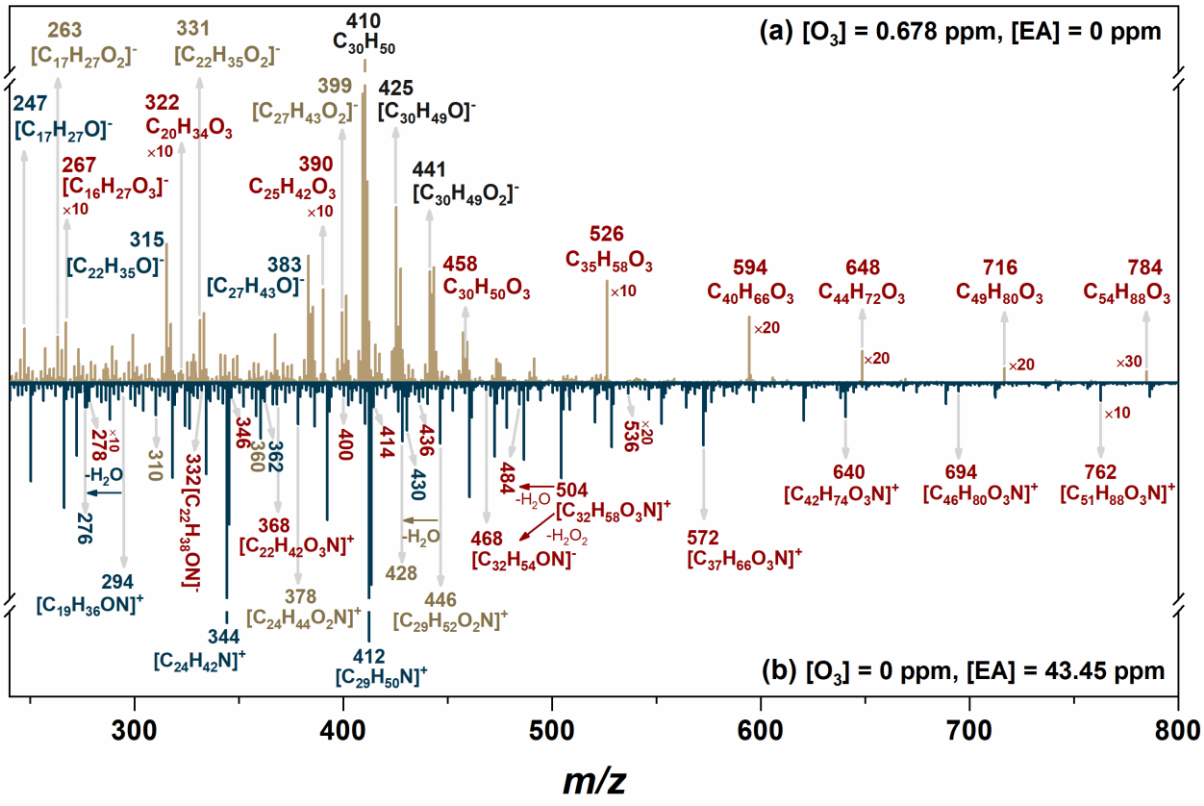

Figure S3. Products distributions from (a) Sqe ozonolysis at 0.678 ppm O_3 in the first flowtube reactor, and (b) subsequent amination reactions with ethylamine ([EA] = 43.45 ppm) in the secondary flowtube reactor.

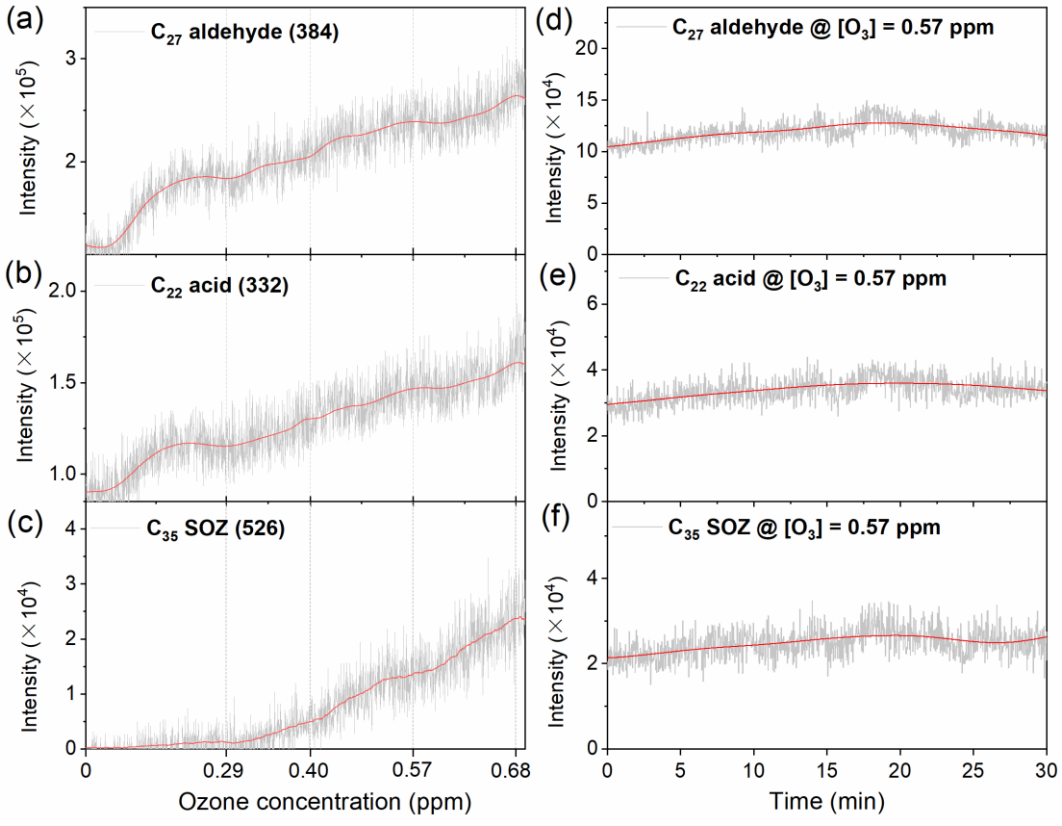

Figure S4. Mass spectral intensities of representative C_{27} aldehyde (*MW* 384), C_{22} carboxylic acid (*MW* 332), and C_{35} SOZ (*MW* 526) in the first flowtube reactor under (a-c) varying O_3 concentrations (0, 0.29, 0.4, 0.57, and 0.68 ppm); as well as (d-f) at fixed O_3 concentration (0.57 ppm).

Figure S5 shows the direct orifice-sampling interface coupled with particle evaporation and photoionization for APPI-HRMS analysis (Liu et al., 2024). The particles flow (800 mL/min) was introduced into the online detection system through a quartz glass tube (235 mm long × 8 mm i.d.), featuring a 0.5 mm sampling orifice. Particles are vaporized by a heater positioned outside the tube (maintained at 180 ℃) ensure particle vaporization prior to ionization. A vacuum ultraviolet (VUV) lamp (PKS106, Heraeus, Ltd.) with a photon energy of 10.6 eV (117 nm) provides soft photoionization, minimizing fragmentations during ionization. The mass resolution of HRMS (Orbitrap Fusion, Thermo Scientific) is 500,000 at *m/z* 200. During the experiments, the MS mode was set to positive polarity. Meanwhile, the ion transfer tube was maintained at 300 ℃. The mass

range from *m/z* 75 to 800 was scanned with a rate of 30 spectra/min, and the resulting data were collected using Xcalibur 4.0 software.

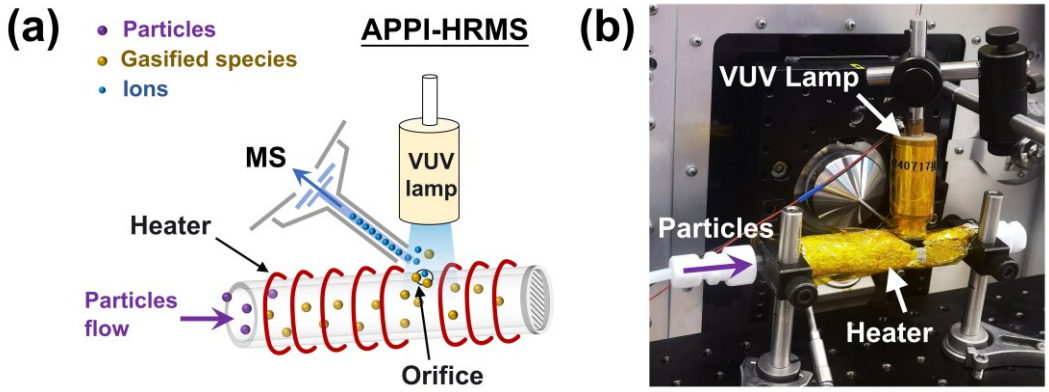

Figure S5. (a) Schematic diagram and (b) photograph of the direct-orifice sampling interface integrated with online APPI-HRMS.(Liu et al., 2024)

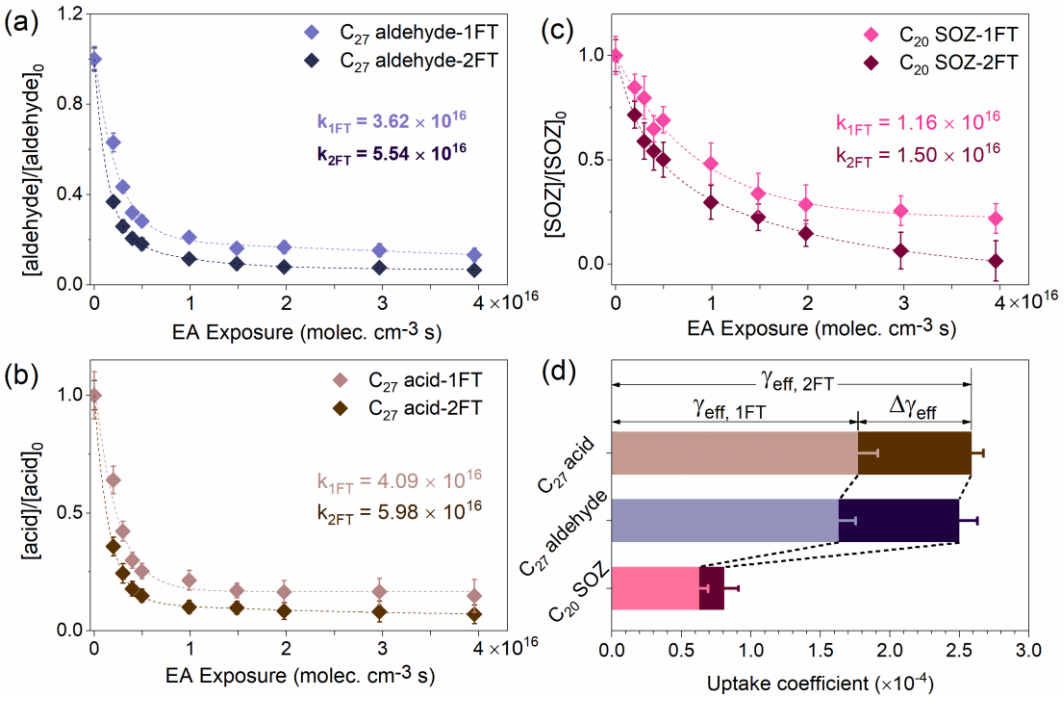

Figure S6. (a-c) The decay kinetics of representative (a) C_{27} aldehyde, (b) C_{27} carboxylic acid, and (c) C_{20} SOZ under control single flowtube experiment (1FT) and tandem flowtube reactor experiment (2FT). The derived decay rates of these organic particles (denoted as k_{1FT} and

k_{2FT}) were used to calculate (d) the differential uptake coefficients ($\Delta\gamma_{eff}$), revealing the net reaction contribution in the secondary flowtube reactor.

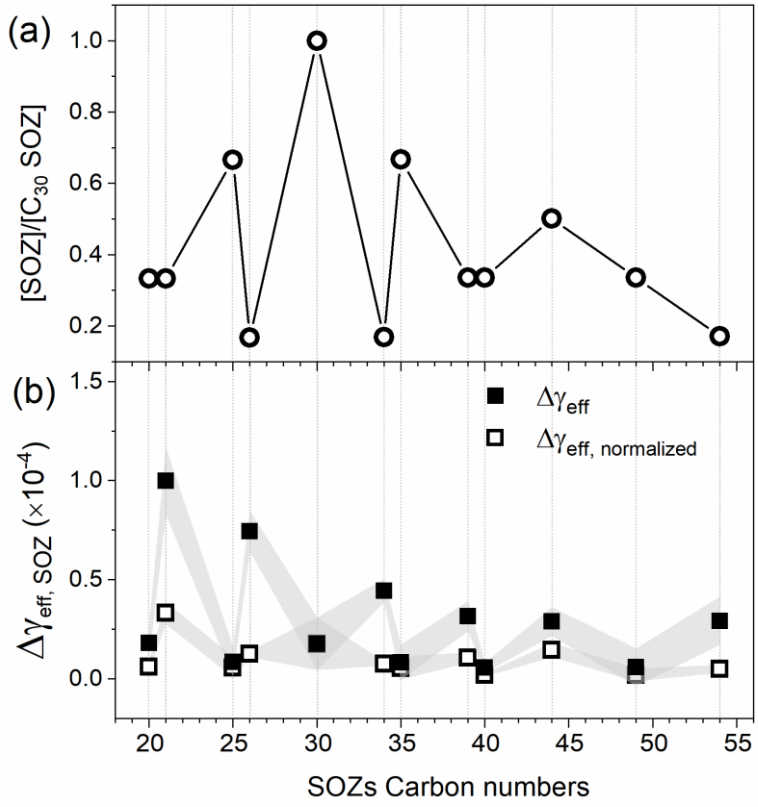

Figure S7. (a) Relative abundances of SOZs normalized to the C_{30} SOZ (maximum concentration) based on data from Ref.(Liu et al., 2024; Heine et al., 2017). (b) Experimentally determined differential uptake coefficients (denoted as $\Delta\gamma_{eff}$) for C_{20} to C_{54} SOZs were normalized by their relative abundances of yield $\Delta\gamma_{eff,\ normalized}$. The reduced differences in $\Delta\gamma_{eff,\ normalized}$ values exhibit compared to original $\Delta\gamma_{eff}$ values demonstrates that the abundance of SOZs influence their heterogeneous reactivity with ethylamine.

Section S2. Reaction mechanisms

This section presents supporting reaction mechanisms, including the ozonolysis reactions of Sqe (Figs. S8-S10), reactions between SOZs with amines (Figs. S11-S13 and Fig. S15), and reactions between C_{17} aldehyde (or carboxylic acid) with ethylamine (Fig. S14).

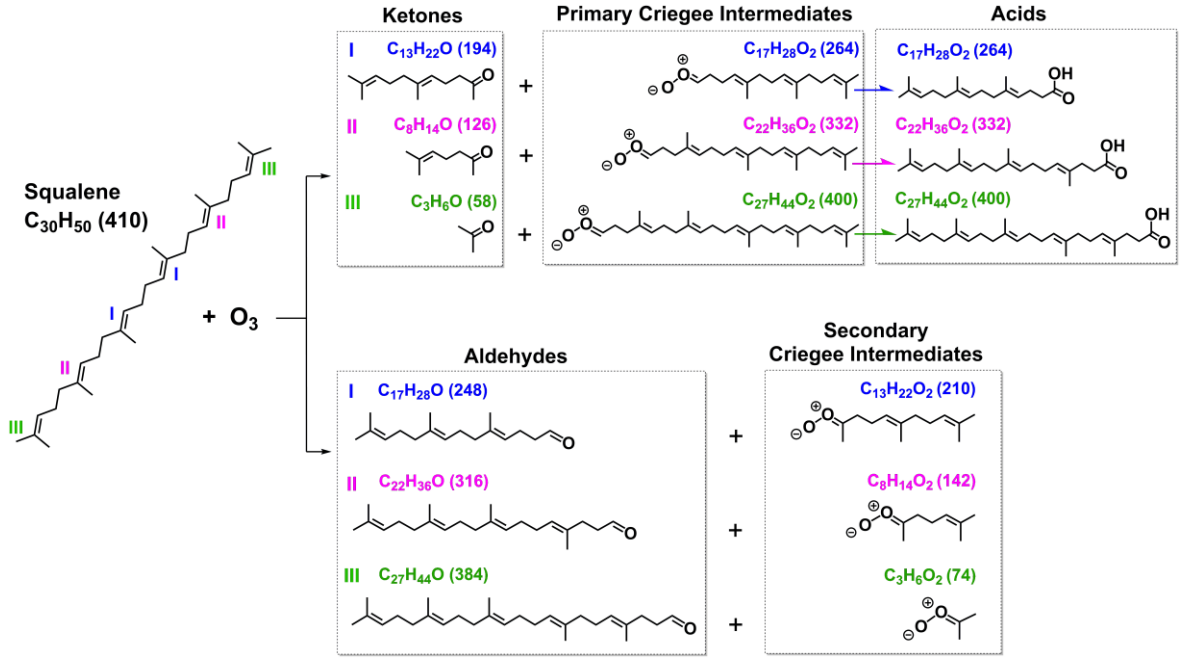

58

59 **Figure S8.** Ozonolysis of squalene (Sqe) yields aldehydes (*MW* 248, 316, and 384), ketones (*MW* 194, 126, and 58), and CIs. The
60 isomerization reactions of primary CIs produce carboxylic acids (*MW* 264, 332, and 400).(Heine et al., 2017)

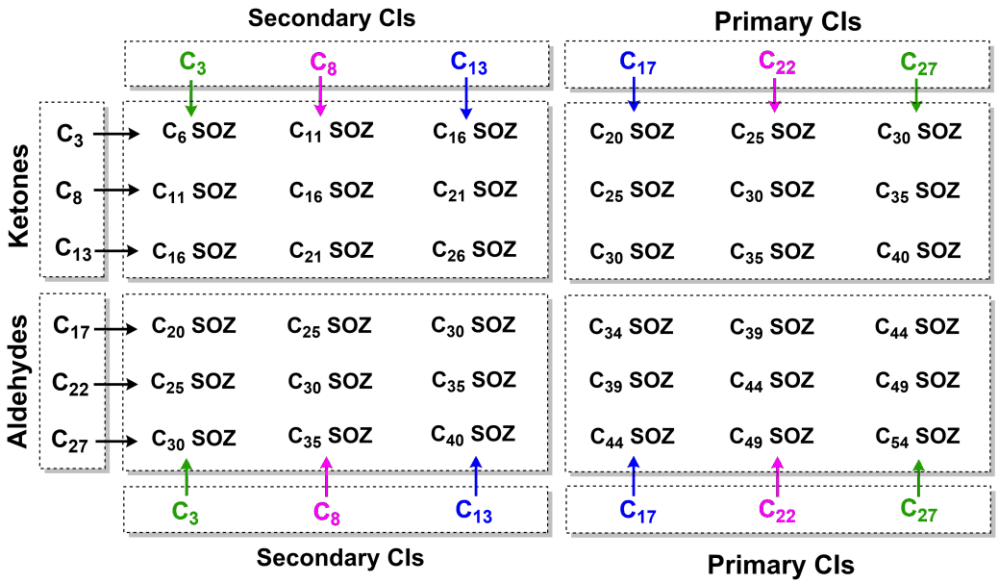

61

62 **Figure S9.** Bimolecular reactions between primary (or secondary) CIs and aldehydes (or ketones) leading to the formation of SOZs.

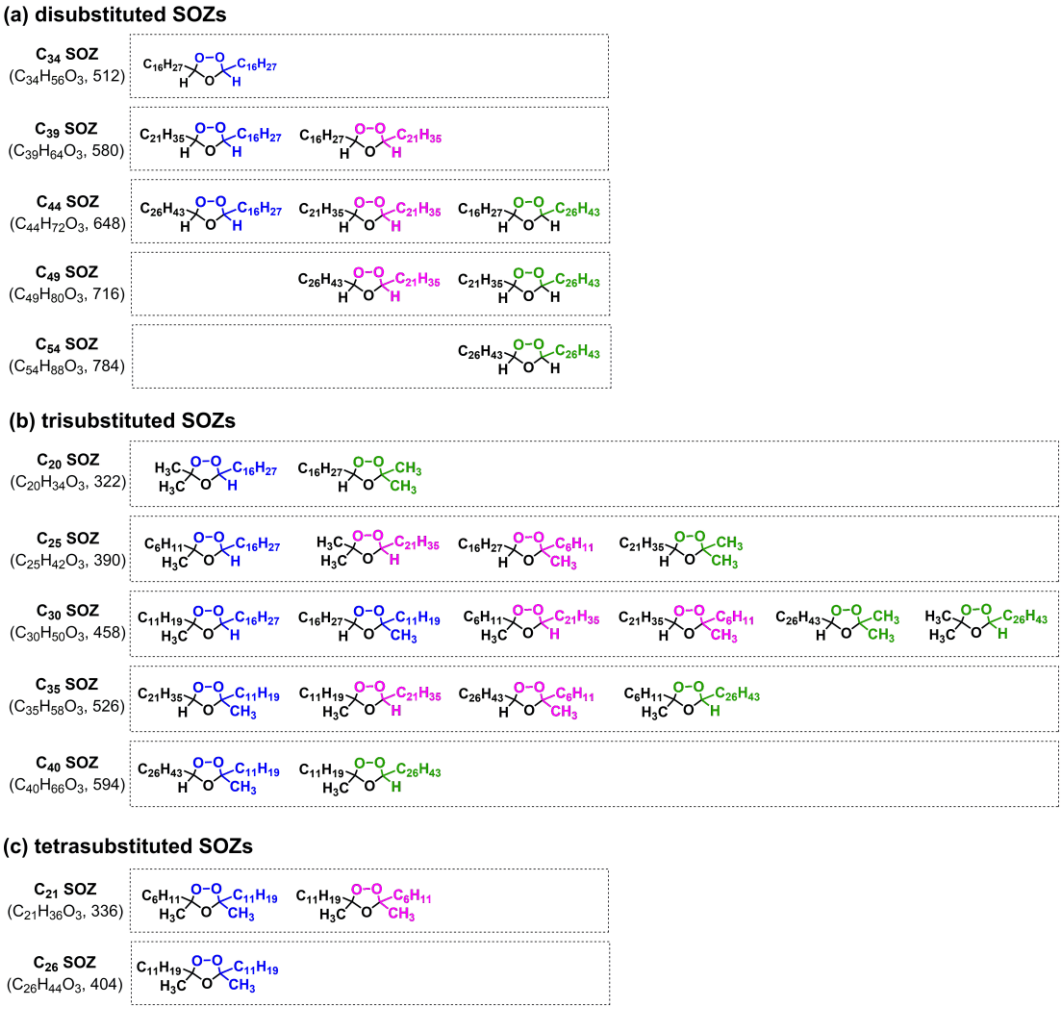

Figure S10. Structural classification of SOZs according to the number of alkyl substituents: (a) disubstituted (C_{34}, C_{39}, C_{44}, C_{49} and C_{54}), (b) trisubstituted (C_{20}, C_{25}, C_{30}, C_{35} and C_{40}), and (c) tetrasubstituted (C_{21} and C_{26}) SOZs.

Figure S11 illustrates established reaction mechanisms of SOZs with amines, highlighting mechanistic controversies (Qiu et al., 2024; Zahardis et al., 2008; Almatarneh et al., 2020; Jørgensen and Gross, 2009; Na et al., 2006). Zahardis et al. (2008) identified a reaction pathway of a C_{18} SOZ with octadecylamine to generate a hydroxyl peroxyamine, which undergoes dehydration to yield nonanal and a C_{27} amide. In contrast, Almatarneh et al. (2020), Jørgensen and Gross (2009), and Na et al. (2006) proposed the formation of amino hydroperoxides in SOZ + amine reactions (Almatarneh et al., 2020; Jørgensen and Gross, 2009). Qiu et al. (2024) characterized a direct amination pathway where cyclic SOZ reacts with ethylamine via

concerted H_2O elimination, producing linear amination product (Fig. S11f). Additional pathways have been also proposed in Refs (Almatarneh et al., 2020; Jørgensen and Gross, 2009; Na et al., 2006) (Figs. S11g and S11h).

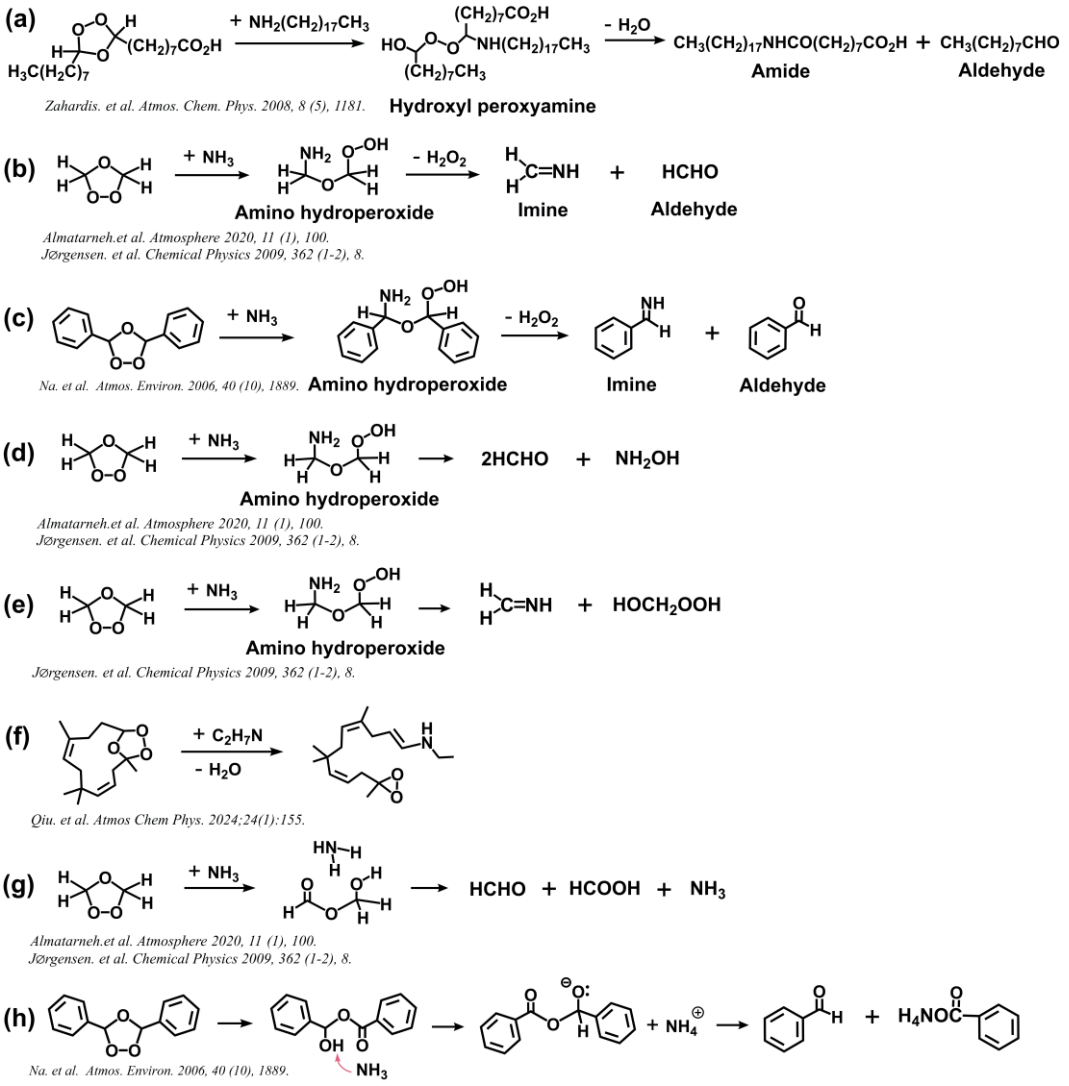

Figure S11. Reaction mechanisms of SOZs with amines as established in previous studies (Qiu et al., 2024; Zahardis et al., 2008; Almatarneh et al., 2020; Jørgensen and Gross, 2009; Na et al., 2006).

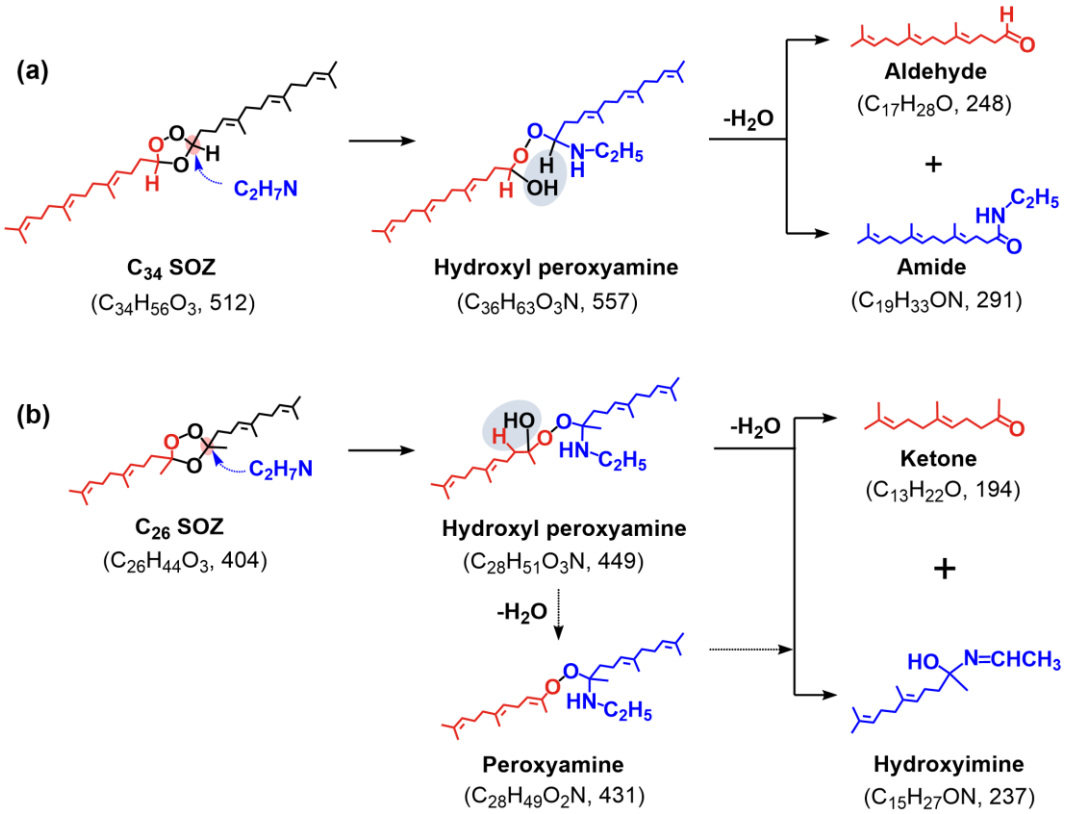

Figure S12. Reaction pathways of representative SOZs with varying alkyl substitution patterns: (a) disubstituted (C_{34}) and (b) tetrasubstituted (C_{26}) SOZs upon exposure to ethylamine (C_2H_7N).

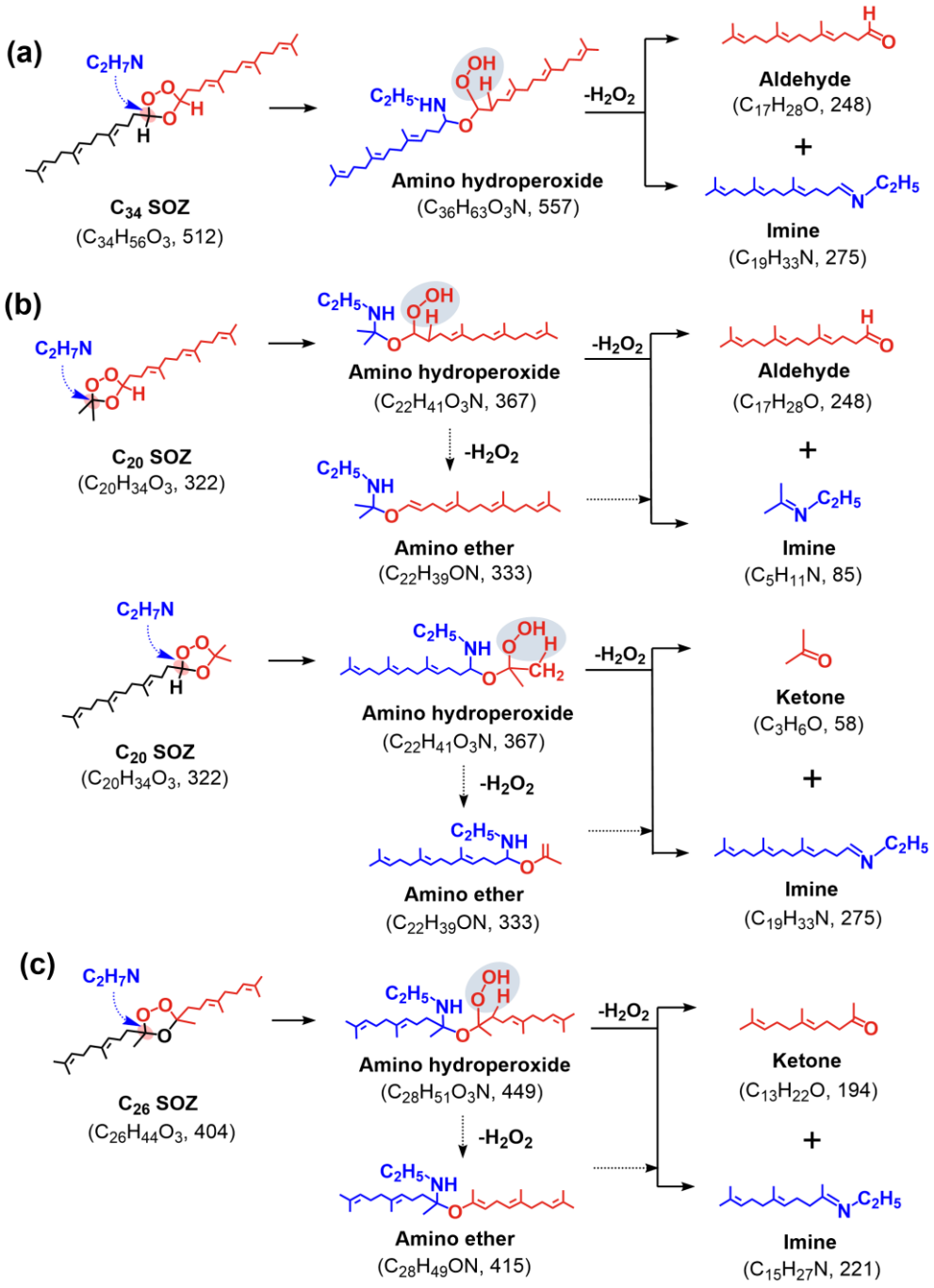

80

81 **Figure S13.** Reaction pathways of representative SOZs with varying alkyl substitution patterns: (a) disubstituted (C_{34}), (b) trisubstituted

82 (C_{20}), and (c) tetrasubstituted (C_{26}) SOZs upon exposure to ethylamine (C_2H_7N).

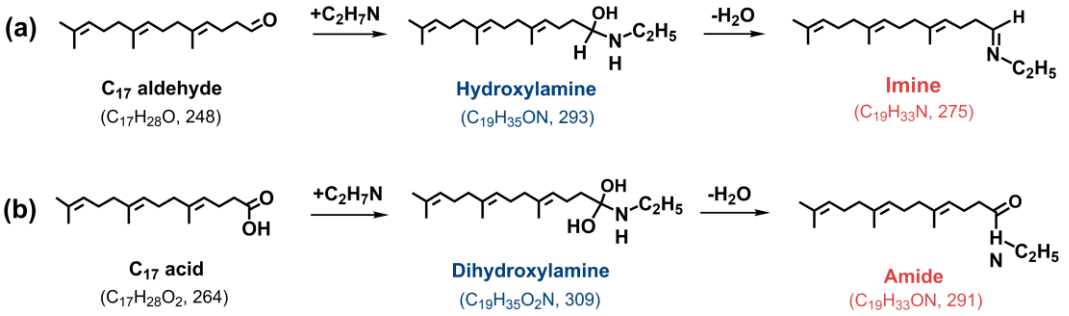

83

84 **Figure S14.** Reaction pathways of (a) C_{17} aldehyde and (b) C_{17} carboxylic acid upon ethylamine exposure.

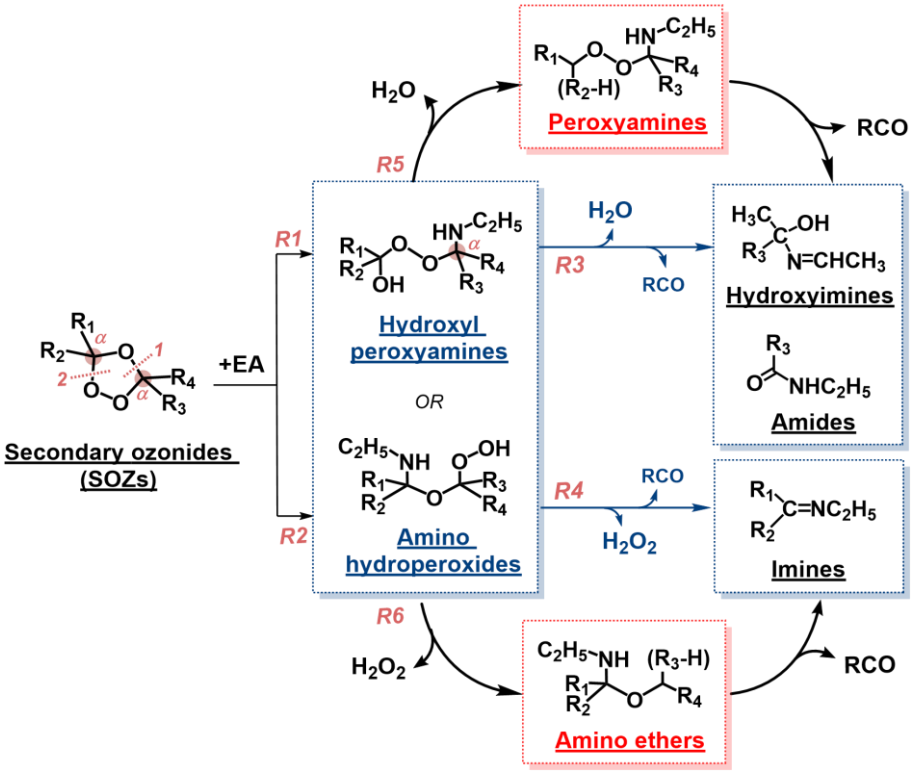

85

86 **Figure S15.** A simplified mechanism of SOZs upon EA exposure.

87

88 **Table S1.** Products observed during the heterogeneous reactions of SOZs, aldehydes, and carboxylic acids with ethylamine.

Representative products	Simplified structures	Formulas	Ions	*m/z*
Hydroxyl peroxyamines or Amino hydroperoxides	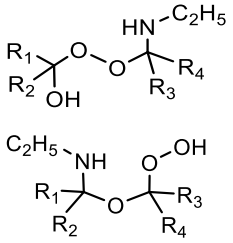	$C_{22}H_{41}O_3N$		368.3154
		$C_{23}H_{43}O_3N$		382.3311
		$C_{27}H_{49}O_3N$		436.3782
		$C_{28}H_{51}O_3N$		450.3939
		$C_{32}H_{57}O_3N$		504.4409
		$C_{36}H_{63}O_3N$	$[M+H]^+$	558.4876
		$C_{37}H_{65}O_3N$		572.5033
		$C_{41}H_{71}O_3N$		626.5497
		$C_{42}H_{73}O_3N$		640.5659
		$C_{46}H_{79}O_3N$		694.6127
		$C_{51}H_{87}O_3N$		762.6746
Peroxyamines	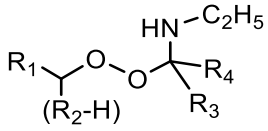	$C_{22}H_{39}O_2N$		348.2896
		$C_{23}H_{41}O_2N$		362.3051
		$C_{27}H_{47}O_2N$	$[M-H]^-$	416.3518
		$C_{28}H_{49}O_2N$		430.3674
		$C_{32}H_{55}O_2N$		484.4144
Amino ethers	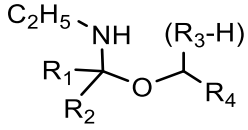	$C_{22}H_{39}ON$		332.2944
		$C_{23}H_{41}ON$		346.3103
		$C_{27}H_{47}ON$	$[M-H]^-$	400.3572
		$C_{28}H_{49}ON$		414.3725
		$C_{32}H_{55}ON$		468.4199

Representative products	Simplified structures	Formulas	Ions	*m/z*
Dihydroxylamines	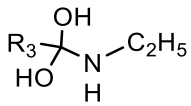	$C_{19}H_{35}O_2N$	$[M+H]^+$	310.2738
		$C_{24}H_{43}O_2N$		378.3364
		$C_{29}H_{51}O_2N$		446.3990
Hydroxylamines	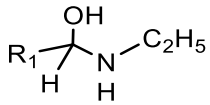	$C_{19}H_{35}ON$	$[M+H]^+$	294.2795
		$C_{24}H_{43}ON$		362.3414
		$C_{29}H_{51}ON$		430.4041
Hydroxyimines	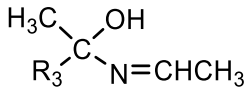	$C_{10}H_{19}ON$	$[M+H]^+$	170.1539
		$C_{15}H_{27}ON$		238.2163
Amides	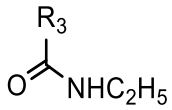	$C_{19}H_{33}ON$	$[M+H]^+$	292.2633
		$C_{24}H_{41}ON$		360.3258
		$C_{29}H_{49}ON$		428.3884
Imines	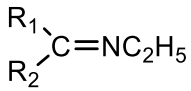	$C_{15}H_{27}N$	$[M+H]^+$	222.2215
		$C_{19}H_{33}N$		276.2684
		$C_{24}H_{41}N$		344.3310
		$C_{29}H_{49}N$		412.3936

89

90

Table S2. Values of $\gamma_{eff,2FT}$, $\gamma_{eff,1FT}$, and $\Delta\gamma_{eff}$ for representative SOZs, carboxylic acids, and aldehydes.

Reactants	Formulas	$\gamma_{eff,2FT}$	$\gamma_{eff,1FT}$	$\Delta\gamma_{eff}$
SOZs	$C_{20}H_{34}O_3$	8.06×10^{-5}	6.24×10^{-5}	1.82×10^{-5}
	$C_{21}H_{36}O_3$	3.30×10^{-4}	2.30×10^{-4}	1.00×10^{-4}
	$C_{25}H_{42}O_3$	3.92×10^{-5}	3.07×10^{-5}	8.50×10^{-6}
	$C_{26}H_{44}O_3$	2.54×10^{-4}	1.79×10^{-4}	7.50×10^{-5}
	$C_{30}H_{50}O_3$	8.60×10^{-5}	6.84×10^{-5}	1.76×10^{-5}
	$C_{34}H_{56}O_3$	1.26×10^{-4}	8.18×10^{-5}	4.42×10^{-5}
	$C_{35}H_{58}O_3$	6.02×10^{-5}	5.20×10^{-5}	8.20×10^{-6}
	$C_{39}H_{64}O_3$	7.31×10^{-5}	4.16×10^{-5}	3.15×10^{-5}
	$C_{40}H_{66}O_3$	2.65×10^{-5}	2.09×10^{-5}	5.60×10^{-6}
	$C_{44}H_{72}O_3$	6.73×10^{-5}	3.85×10^{-5}	2.88×10^{-5}
	$C_{49}H_{80}O_3$	8.37×10^{-5}	7.80×10^{-5}	5.70×10^{-6}
	$C_{54}H_{88}O_3$	1.03×10^{-4}	7.41×10^{-5}	2.89×10^{-5}
Carboxylic acids	$C_{17}H_{28}O_2$	5.44×10^{-4}	3.14×10^{-4}	2.30×10^{-4}
	$C_{22}H_{36}O_2$	3.27×10^{-4}	1.93×10^{-4}	1.33×10^{-4}
	$C_{27}H_{44}O_2$	2.59×10^{-4}	1.77×10^{-4}	8.19×10^{-5}
Aldehydes	$C_{17}H_{28}O$	4.55×10^{-4}	3.26×10^{-4}	1.30×10^{-4}
	$C_{22}H_{36}O$	2.85×10^{-4}	1.80×10^{-4}	1.05×10^{-4}
	$C_{27}H_{44}O$	2.50×10^{-4}	1.63×10^{-4}	8.67×10^{-5}

SI References

Almatarneh, M. H., Alrebei, S. F., Altarawneh, M., Zhao, Y., and Abu-Saleh, A. A.-A.: Computational study of the dissociation reactions of secondary ozonide, Atmosphere., 11, 100-110, https://doi.org/10.3390/atmos11010100, 2020.

Heine, N., Houle, F. A., and Wilson, K. R.: Connecting the elementary reaction pathways of criegee intermediates to the chemical erosion of squalene interfaces during ozonolysis, Environ. Sci. Technol., 51, 13740-13748, https://doi.org/10.1021/acs.est.7b04197, 2017.

Jørgensen, S. and Gross, A.: Theoretical investigation of reactions between ammonia and precursors from the ozonolysis of ethene, Chem. Phys., 362, 8-15, https://doi.org/10.1016/j.chemphys.2009.05.020, 2009.

Liu, P., Gao, J., Xiao, X., Yuan, W., Zhou, Z., Qi, F., and Zeng, M.: Investigating the kinetics of heterogeneous lipid ozonolysis by an online photoionization high-resolution mass spectrometry technique, Anal. Chem., 96, 19576-19584, https://doi.org/10.1021/acs.analchem.4c04404, 2024.

Na, K., Song, C., and Cockeriii, D.: Formation of secondary organic aerosol from the reaction of styrene with ozone in the presence and absence of ammonia and water, Atmos. Environ., 40, 1889-1900, https://doi.org/10.1016/j.atmosenv.2005.10.063, 2006.

Qiu, J., Shen, X., Chen, J., Li, G., and An, T.: A possible unaccounted source of nitrogen-containing compound formation in aerosols: amines reacting with secondary ozonides, Atmos. Chem. Phys., 24, 155-166, https://doi.org/10.5194/acp-24-155-2024, 2024.

Zahardis, J., Geddes, S., and Petrucci, G. A.: The ozonolysis of primary aliphatic amines in fine particles, Atmos. Chem. Phys., 8, 1181-1194, https://doi.org/10.5194/acp-8-1181-2008, 2008.